Towards Space-Time Incoherent Transmitter Design for Millimeter-Wave Imaging

Stavros Vakalis, *Student Member, IEEE*, Daniel Chen, *Student Member, IEEE*, and Jeffrey A. Nanzer, *Senior Member, IEEE*

***Abstract*—It was recently demonstrated that microwave and millimeter-wave imagery can be obtained using multiple noise transmitters to illuminate the scene with incoherent space-time varying fields and a sparse receiving interferometric array. Incoherent imaging has a number of benefits compared to coherent imaging, including no required synchronization between the transmitters and receivers, and fast processing that does not require solving an inverse problem. In this paper we present a method for characterizing the spatial incoherence of the transmitted signals in an incoherent millimeter-wave imager. We demonstrate theoretically, and experimentally, the characterization of the transmitted radiation spatial coherence as a function of number of noise transmitters in a 37 GHz imaging system.**

***Index Terms*—Distributed antenna arrays, incoherent imaging, interferometric imaging, space-time**

I. Introduction

INCOHERENT space-time fields have long been used in optical imaging, with flashlight illumination in optical photography a prominent example. In situations where there is no ambient light in a room, the flashlight illumination can compensate for this low visibility condition. Such incoherent illumination has not traditionally been used for imaging in the microwave and millimeter-wave range (3-300 GHz). Most imaging techniques in these frequencies utilize mechanically or electronically scanning arrays and coherent illumination [1]–[3]. Generally, these techniques cannot produce real-time imagery due to the extended time required to scan a scene in the spatial domain. Computational imaging can reduce the number of receivers and data acquisition time required to reconstruct the images using coherent pseudo-random space-time modulations with minimal mutual information between measurement modes [4], [5]. However, such techniques require significant signal processing, leading to latencies that are infeasible for real-time imaging. Furthermore, these approaches require precise knowledge of the pseudo-random space-time modulation, which necessitates additional and potentially frequent calibration. Passive millimeter-wave imaging systems capture incoherent thermal radiation emitted by people and objects in a scene, and have been implemented with sparse receiving arrays for Fourier-domain imaging. However, thermal radiation is very low in power at microwave and millimeter-wave frequencies, necessitating high sensitivity through large signal gains, wide receiver bandwidth, and accurately calibrated components, leading to significant costs [6]–[8].

To overcome the sensitivity limitations of passive imagers, the authors recently introduced a new computational imaging technique called active incoherent millimeter-wave (AIM) imaging that leverages incoherent signal transmission and interferometric imaging for real-time imaging [9]–[11]. The radiation emitted or scattered by a scene must be incoherent for successful interferometric image reconstruction according to the Van-Cittert Zernike theorem [12], [13]; thermal radiation satisfies this requirement, but traditional coherent illumination does not. Our prior work has shown that illuminating the scene with multiple noise transmitters generates a sufficiently incoherent signal at the image plane to obtain imagery with an interferometric receiver [9]. The use of active illumination serves to increase the signal-to-noise ratio significantly compared to passive imagers, thus high-gain wide-bandwidth receivers are not required, leading to significantly lower overall system cost. Interferometric arrays are furthermore inherently sparse [10], thus reducing the total amount of hardware in comparison to a traditional phased array. They are also resistant to element failures [11], making them ideal for applications where lower-cost, uninterrupted operation is desired. Another important advantage of AIM imaging and other incoherent imaging techniques (e.g. [14]) compared to coherent approaches is that the exact knowledge of the transmitter space-time modulation is not needed. The significance of this becomes apparent considering the impact of the necessary knowledge to implement other sparse array imaging techniques such as multiple-input multiple-output (MIMO), where the individual code on each transmitter must be known and appropriately coordinated among all receivers in the array. In AIM imaging, no synchronization is necessary between transmitters and receivers. The received signals are cross-correlated, and image formation is then obtained directly using an inverse Fourier transform (IFT).

In this paper, we present and experimentally demonstrate a technique for measuring the spatial coherence in the image plane of signals emitted by a set of incoherent transmitters. Currently, no metrics exist for characterizing the image plane coherence in AIM imaging systems, meaning that transmitter design has proceeded in heuristic form. This work provides a fundamental first step towards a comprehensive design approach for AIM transmitter arrays. We present a multi-element measurement concept and demonstrate through experiment with a 37 GHz system the spatial coherence of transmitters with one, two, and three incoherent emitters.

Manuscript received 2020.

This material is based upon work supported by the National Science Foundation under grant 1708820. *(Corresponding author: Jeffrey A. Nanzer)*

The authors are with the Department of Electrical and Computer Engineering, Michigan State University, East Lansing, MI 48824 USA (email: vakaliss@msu.edu, chendan7@msu.edu, nanzer@msu.edu).

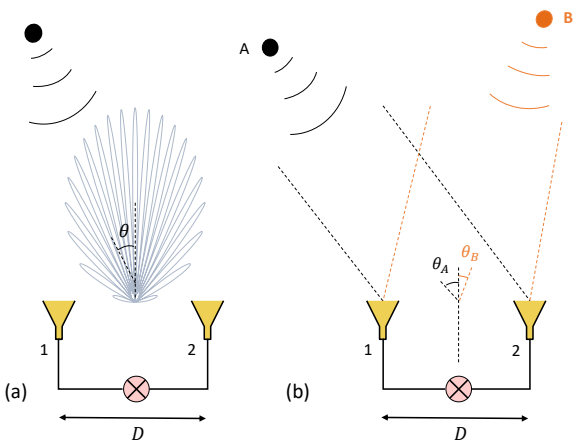

Fig. 1. (a) Point source response of a correlation interferometer. (b) Correlation interferometer geometry observing two point sources A and B.

II. Active Incoherent Millimeter-Wave Imaging

Interferometric antenna arrays perform image reconstruction by capturing samples of the scene visibility $V(u)$, which is the Fourier transform of the scene intensity I. This set of samples is called sampled visibility $V_s(u)$, and the reconstructed scene intensity I_r in one dimension is given by

$$I_r(\gamma) = \sum_{n}^{N} V_s(u_n) e^{-j2\pi u_n \gamma} \tag{1}$$

where N is the number of visibility samples, and $\gamma = \sin\theta$. While we consider one-dimensional signals in this work, the process directly extends to two dimensions [9], [15]. Interferometric arrays measure spatial frequency information by cross-correlating the signals received at different elements in the array. The interference pattern generated by two widely-spaced elements forming a correlation interferometer, shown in Fig. 1a, defines a specific spatial frequency u_m (rad^{-1}), and the cross-correlation of the signals between the two elements corresponds to one sample of the visibility. The geometric time delay between the two antennas $\tau_g = \frac{D}{c}\sin\theta$ for wavefront propagation speed c, a target at angle θ and the antenna baseline D gives a cross-correlation response

$$r(\theta) = \langle V_1 V_2 \rangle = \langle \cos(2\pi f_c t)\cos[2\pi f_c (t-\tau_g)] \rangle \tag{2}$$

where f_c is the carrier frequency. The angle brackets indicate multiplication and integration (low-pass filtering), resulting in

$$r(\theta) = \frac{1}{2}\cos\left(\frac{2\pi}{\lambda} D \sin\theta\right) \tag{3}$$

where $\lambda = c/f_c$ is the corresponding wavelength. The result is a fringe response with a number of lobes equal to the corresponding spatial frequency $u_m = D/\lambda$.

The importance of spatial incoherence at the image plane can be seen by considering two point sources as shown in Fig. 1b, where the two receiver voltages can be expressed as

$$V_1 = s_{1A} + s_{1B} + n_1 \tag{4}$$

$$V_2 = s_{2A} + s_{2B} + n_2 \tag{5}$$

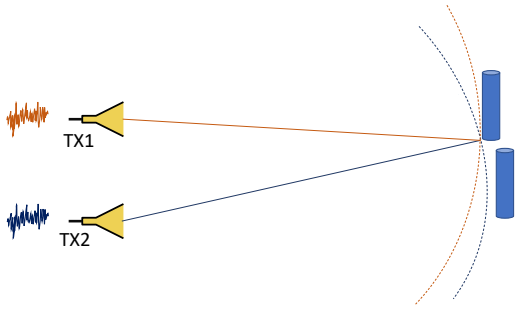

Fig. 2. Two noise sources illuminating two targets.

where s_{iA}, s_{iB} are the terms that represent the response of the i^{th} element due to the point sources A and B respectively, and n_i is noise. The output voltage, after cross-correlating the two receiver responses, can be given by

$$\begin{aligned} V_{out} &= \langle V_1 V_2 \rangle \\ &= \langle s_{1A} s_{2A} \rangle + \langle s_{1B} s_{2B} \rangle + \langle s_{1A} s_{2B} \rangle + \langle s_{1B} s_{2A} \rangle \end{aligned} \tag{6}$$

The noise terms, being completely uncorrelated, tend to zero when multiplied and integrated, leaving only the responses from the two point sources. The first two terms in (6) represent the cross-correlation of the individual signals from the two points at each receiver, and thus are points in the sampled visibility. The second two terms are cross-correlations that remain if the signals scattered off points A and B are correlated. Ideally, these signals will be completely uncorrelated and will tend to zero as well, leaving

$$V_{out} = \langle V_1 V_2 \rangle \approx \langle s_{1A} s_{2A} \rangle + \langle s_{1B} s_{2B} \rangle \tag{7}$$

In practice, the transmitted signals, and thus the signals scattered off A and B will have some non-zero correlation, and the residual cross terms $\langle s_{1A} s_{2B} \rangle$ and $\langle s_{1B} s_{2A} \rangle$ will be present, corrupting the visibility sample and degrading the reconstructed image. In the following, we present a method of characterizing the incoherence of the signals emitted by the transmitting array in the spatial domain.

III. Spatial Coherence of Noise Transmitters

The superposition of two completely incoherent signals transmitted from two different points in space manifests as a unique signal across space and time. The degree to which two points in space are correlated impacts the residual terms in (6) and therefore the image reconstruction quality. The spatial dependence from the superposition of the two signals, such as shown in Fig. 2, can be analyzed by considering the signals to be emitted by two point radiators. The two transmitters generate two spherical waves whose information is completely correlated along the surface of the wave. Two circles with different centers in a 2-D plane can have up to two intersecting points. Due to the symmetry of our case it will be one intersecting point in the front and one in the back of the array. Using directive antennas the ambiguous "image" point located behind the antennas can be ignored. Therefore, the intersection of the waves from separate equal

amplitude transmitters represents a unique point, as shown in Fig. 2. The argument extends directly to a 3-D space, where three spheres emitted by the sources intersect. With the same front-back symmetry and directive antennas, an unambiguous measurement is thus obtained in 3-D using three emitters.

The intersections of the wavefronts represent points of unique illumination, however even completely uncorrelated transmit signals will display some amount of correlation at the image plane, depending on the number of transmitters. This is because the information at the intersection contains information from all the transmitters, which is constant across the wavefronts; hence for a two-element transmitter as in Fig. 2, the information everywhere along the red wavefront from TX1 is also present at the intersection. The signal at the intersection is therefore correlated with the information at every point along the wavefront by $\frac{1}{2}$, because the contribution from one out of the two transmitters is identical for all these points. Designating an image plane extending vertically across the scene, there will thus be one other point in the plane that is 50% correlated with the signal at the intersection. Extending this concept, by using N trasmitters, any two points in the image plane will have at most $\frac{100}{N}\%$ correlation. A useful metric to quantify the similarity of the electric field E at two points 1 and 2 is the complex degree of coherence [12], [13], [16] which in optics and radio astronomy can be found through the following formula

$$\Gamma_{12}(\tau) = \lim_{T\to\infty} \frac{1}{2T} \int_{-T}^{T} E_1(t) E_2^*(t-\tau)\, dt \tag{8}$$

where T is the integration time. Usually when measuring spatial coherence between two different points we refer to their fields at exactly the same time, so we can set $\tau = 0$. Temporal coherence is also critical for interferometric imaging and radar systems in general [17], [18], however in this work the spatial coherence is of greater importance. The integral in Eq. 8 can be written for a set of N points in discretized form as the mutual coherence matrix γ [19], [20], each entry of which γ_{ij} is the dot product of the point responses ϵ_i and ϵ_j,

$$\gamma_{ij} = \frac{|\epsilon_i \epsilon_j^H|}{||\epsilon_i|| ||\epsilon_j||} \tag{9}$$

where $1 \leq i, j \leq N$. A dot product γ_{ij} close to 1 indicates high spatial coherence, while γ_{ij} close to 0 indicates low coherence (incoherence); intermediate values $0 < \gamma_{ij} < 1$ correspond to partial coherence. In the example of Fig. 2 two points in the same circle arc will have $\gamma_{ij} = 1/2$, and for N transmitters $\gamma_{ij} = 1/N$.

IV. Modeling Coherence from Multiple Sources

In a two-dimensional space the field from N noise sources at a carrier frequency f_c with bandwidth Δf can be found as a function of time as

$$E(x,y,t) = \sum_{i=1}^{N} \int_{f_c - \frac{\Delta f}{2}}^{f_c + \frac{\Delta f}{2}} a_i(f) e^{j2\pi f t + \phi_i(t)} \cdot \frac{\delta(t - R_i/c)}{R_i}\, df \tag{10}$$

where $\alpha_i(f)$ is the amplitude of the signal emitted by antenna i, $\phi_i(t)$ is the signal phase, and $R_i = \sqrt{(x-x_i)^2 + (y-y_i)^2}$ is the distance of each point (x, y) from the transmitters locations (x_i, y_i). We evaluated the mutual coherence from a set of three 37 GHz incoherent sources TX1, TX2, and TX3 simulated in MATLAB and placed in a rectangular grid (x,y) at locations (-0.1,0), (0.1,0), and (0.15,0) meters, respectively. The image segment where mutual coherence was measured was set to be the line connecting the points (-1,2.61) and (1,2.61). The simulated mutual coherence is shown in Fig. 3 where γ is plotted for all three transmitters in Fig. 3a and for TX1 and TX2 in Fig. 3b. The matrices are symmetric and its diagonal elements are unity because each spatial point is self-coherent. Most of the terms γ_{ij} where $i \neq j$, representing the points outside of the wavefront arc, are negligible because of the spatial incoherence, however in Fig. 3a three partial coherence lines appear with amplitude $\frac{1}{3}$, and in Fig. 3b two partial coherence lines show up with amplitude $\frac{1}{2}$. These lines are due to the intersection of the circular wavefront coming from the three sources with the line segment, and do not indicate the antenna locations. Using N incoherent transmitters will result in N partial coherence lines in the image plane with $\gamma_{ij} = \frac{1}{N}$. As the number of element increases more partial coherence lines will appear but with lower amplitude. Thus, by increasing the number of transmitters, points of ambiguity are significantly reduced at the image plane. The next section presents an experimental verification of the image plane coherence.

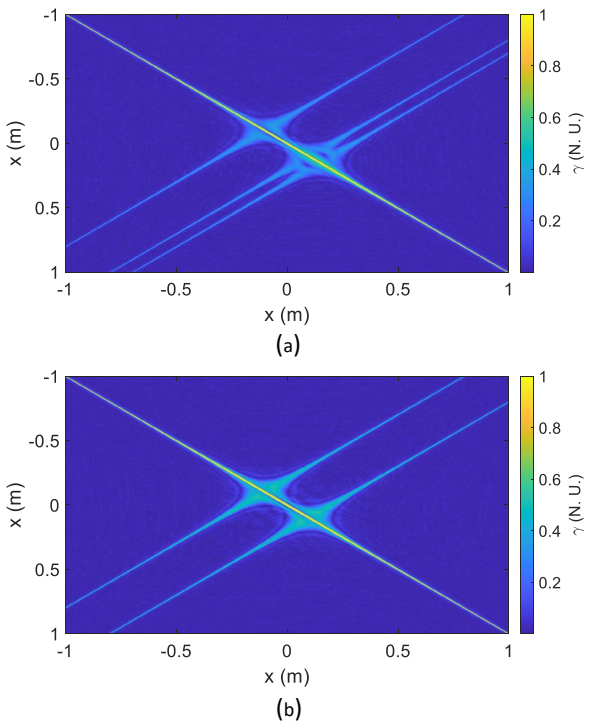

Fig. 3. Simulation of the mutual coherence matrices γ at a 1-D image plane for (a) three incoherent sources and (b) two incoherent sources. The unity diagonal elements represent the self-coherence of every point. The additional lines represent partial coherence from the emitter wavefronts, with coherence of $\frac{1}{3}$ for $N = 3$ and $\frac{1}{2}$ for $N = 2$. Generally, N transmitters yield N partial coherence lines with amplitude $\frac{1}{N}$

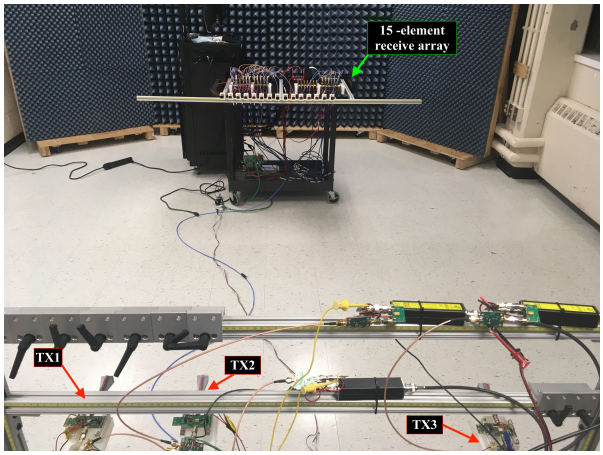

Fig. 4. Experimental setup for measuring the mutual coherence on a line segment using 15 receivers and three transmitters.

V. Experimental Measurements of Partial Coherence from Incoherent Sources

Experimental measurements were conducted inside a semi-anechoic environment at a carrier frequency of 37 GHz. 15 dBi 3D-printed horn antennas were used for both transmitters and receivers. For the receivers each antenna was followed by a 20 dB gain Analog Devices (ADI) HMC1040LP3CE low-noise amplifier (LNA) before being downconverted to baseband using a 37-44 GHz quadrature downconverter (ADI HMC6789BLC5A). Their outputs were captured using two ATS9416 14 bit, 100 MS/s, AlazarTech waveform digitizers installed on a computer in master-slave mode. The three transmitters consisted of three calibrated 15 dB Excess Noise Ratio (ENR) noise sources which were amplified at baseband, and then upconverted to 37 GHz using ADI HMC6787ALC5A 37-40 GHz upconverters. Three power amplifiers ADI HMC7229LS6 were used to amplify the 37 GHz signal to a transmit power of -8 dBm.

The experimental configuration can be seen in Fig. 4. The receive array consisted of 15 antennas spaced uniformly in 5 cm increments seen at the top of Fig. 4. Receive elements are numbered from 1 to 15 with the receiver 1 being the receiver at the top right side of the picture, while receiver 15 is the one at the top left side of the picture. The sampling rate was 100 MS/s and the integration time 1.6 ms. The receivers were calibrated using redundant spacings [15], [21]. The distance between transmitters and receivers was 2.62 m. TX1 and TX2 were spaced 0.2 m apart, while TX2 and TX3 were spaced 0.51 m apart. The locations here are sparse compared to the discretized grid in the simulations of the previous section, however they are a useful indicator for how the partial coherence in the image plane behaves as a function of number of transmitters and transmit element spacings. The results can be seen in Fig. 4 for (a) all three noise sources, (b) TX1 and TX3, and (c) only TX1 transmitting. The matrix is normalized columnwise and due to residual calibration errors is not perfectly symmetric. It can be seen that three noise sources in Fig. 4a produce significantly more incoherent radiation than the two noise sources in Fig. 4b, where the partial coherence

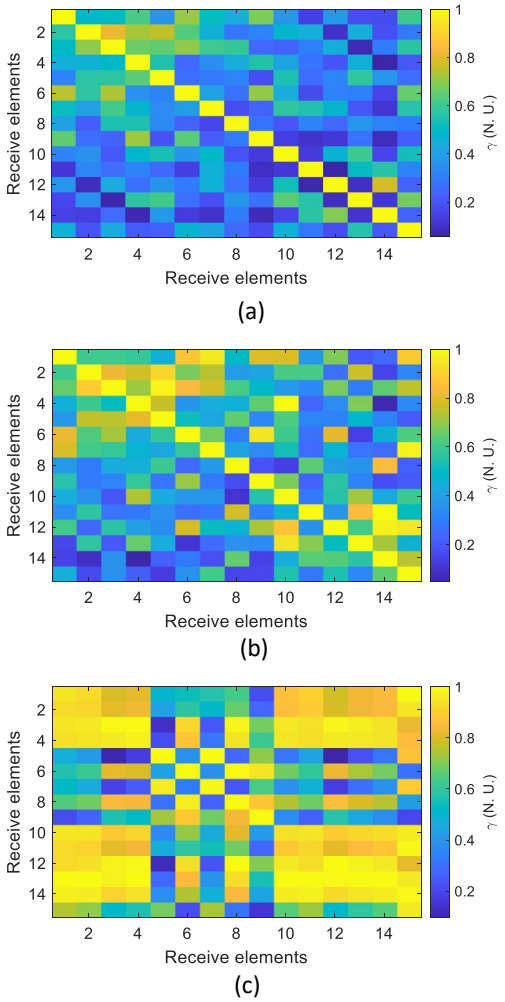

Fig. 5. Experimentally measured coherence matrices γ using (a) three incoherent transmitters, (b) two incoherent transmitters, and (c) one incoherent transmitter, showing lower mutual coherence (higher incoherence) as the number of emitters increases.

lines that are significantly higher than the image noise floor, which is due to hardware imperfections and variations between the transmitter power levels, start to appear. Fig. 4c shows that a single noise transmitter produces significant correlation in the scene, thus active interferometric imaging requires multiple incoherent transmitters when imaging in even 1-D. While the measurement was not optimized to mitigate multipath or other environmental reflections, there is nonetheless significant agreement between simulation and measurement.

VI. Conclusion

Analysis of the coherence in the image plane from a set of transmitters represents a significant step towards transmit array design in AIM imaging. In this work, we demonstrated the use of mutual coherence to determine the impacts of image-plane spatial coherence as a function of the number of transmitters. This approach can be used in the design of active incoherent imaging systems, and also in the analysis of non-cooperative emitters, such as WiFi signals, which may also be used for incoherent imaging [22].

REFERENCES

[1] A. Clemente *et al.*, "Wideband 400-element electronically reconfigurable transmitarray in x band," *IEEE Trans. Antennas Propag.*, vol. 61, no. 10, pp. 5017–5027, Oct 2013.

[2] D. M. Sheen, D. L. McMakin, and T. E. Hall, "Three-dimensional millimeter-wave imaging for concealed weapon detection," *IEEE Trans. Microw. Theory Techn.*, vol. 49, no. 9, pp. 1581–1592, Sep 2001.

[3] P. C. Theofanopoulos and G. C. Trichopoulos, "Modeling of mmw and thz imaging systems using conjugate field coupling," *IEEE Antennas Wireless Propag. Lett.*, vol. 17, no. 2, pp. 213–216, 2018.

[4] M. F. Imani *et al.*, "Review of metasurface antennas for computational microwave imaging," *IEEE Trans. Antennas Propag.*, pp. 1–1, 2020.

[5] J. A. Martinez Lorenzo, J. Heredia Juesas, and W. Blackwell, "A single-transceiver compressive reflector antenna for high-sensing-capacity imaging," *IEEE Antennas Wireless Propag. Lett.*, vol. 15, pp. 968–971, 2016.

[6] L. Yujiri, M. Shoucri, and P. Moffa, "Passive millimeter wave imaging," *IEEE Microw. Mag.*, vol. 4, no. 3, pp. 39–50, Sept 2003.

[7] A. V. Diebold *et al.*, "Passive microwave spectral imaging with dynamic metasurface apertures," *Optica*, vol. 7, no. 5, pp. 527–536, May 2020. [Online]. Available: http://www.osapublishing.org/optica/abstract.cfm?URI=optica-7-5-527

[8] S. Abid *et al.*, "Enhancing millimeter-wave computational interferometric imaging," *IEEE Access*, vol. 8, pp. 101 416–101 425, 2020.

[9] S. Vakalis and J. A. Nanzer, "Microwave imaging using noise signals," *IEEE Trans. Microw. Theory Techn.*, vol. 66, no. 12, pp. 5842–5851, Dec 2018.

[10] ——, "Analysis of array sparsity in active incoherent microwave imaging," *IEEE Geosci. Remote Sens. Lett.*, vol. 17, no. 1, pp. 57–61, Jan 2020.

[11] ——, "Analysis of element failures in active incoherent microwave imaging arrays using noise signals," *IEEE Microw. Wireless Compon. Lett.*, vol. 29, no. 2, pp. 161–163, Feb 2019.

[12] A. R. Thompson, J. M. Moran, and G. W. Swenson, *Interferometry and Synthesis in Radio Astronomy*. John Wiley and Sons, 2001.

[13] M. Born and E. Wolf, *Principles of optics*. Cambridge Univ. Pr., 1999.

[14] A. V. Diebold *et al.*, "Phaseless coherent and incoherent microwave ghost imaging with dynamic metasurface apertures," *Optica*, vol. 5, no. 12, pp. 1529–1541, Dec 2018.

[15] S. Vakalis *et al.*, "Experimental demonstration and calibration of a 16-element active incoherent millimeter-wave imaging array," *IEEE Trans. Microw. Theory Techn.*, pp. 1–1, 2020.

[16] Y. Shao *et al.*, "Spatial coherence measurement and partially coherent diffractive imaging using self-referencing holography," *Opt. Express*, vol. 26, no. 4, pp. 4479–4490, Feb 2018. [Online]. Available: http://www.opticsexpress.org/abstract.cfm?URI=oe-26-4-4479

[17] R. Komissarov *et al.*, "Partially coherent radar unties range resolution from bandwidth limitations," *Nature Commun.*, vol. 10, no. 1423, Dec. 2019.

[18] R. M. Narayanan and M. Dawood, "Doppler estimation using a coherent ultrawide-band random noise radar," *IEEE Trans. Antennas Propag.*, vol. 48, no. 6, pp. 868–878, 2000.

[19] R. Obermeier and J. A. Martinez-Lorenzo, "Sensing matrix design via mutual coherence minimization for electromagnetic compressive imaging applications," *IEEE Trans. Comput. Imag.*, vol. 3, no. 2, pp. 217–229, June 2017.

[20] D. L. Donoho and M. Elad, "Optimally sparse representation in general (nonorthogonal) dictionaries via l1 minimization," *Proceedings of the National Academy of Sciences*, vol. 100, no. 5, pp. 2197–2202, 2003. [Online]. Available: https://www.pnas.org/content/100/5/2197

[21] M. H. Wieringa, "An investigation of the telescope based calibration methods 'redundancy' and 'self-cal'," *Experimental Astronomy*, vol. 2, no. 4, pp. 203–225, Jul 1992. [Online]. Available: https://doi.org/10.1007/BF00420576

[22] S. Vakalis, L. Gong, and J. A. Nanzer, "Imaging with wifi," *IEEE Access*, vol. 7, pp. 28 616–28 624, 2019.